JOURNAL OF GEOPHYSICAL RESEARCH, VOL. 101, NO. B2, PAGES 2815–2834, FEBRUARY 10, 1996

Deconvolution of long-core paleomagnetic data of Ocean Drilling Program by Akaike's Bayesian Information Criterion minimization

Hirokuni Oda[1]

Department of Geology and Mineralogy, Kyoto University, Kyoto, Japan

Hidetoshi Shibuya

Department of Earth Science, College of Integrated Arts and Sciences, University of Osaka Prefecture, Sakai, Japan

Abstract. Deconvolution of long-core paleomagnetic data of the Ocean Drilling Program (ODP) was developed based on Bayesian statistics. Samples of deep-sea sediments obtained by drilling with an advanced piston corer are subjected to pass-through measurements by a cryogenic magnetometer aboard the ODP's research vessel (*Joides Resolution*) which provide continuous paleomagnetic records. Deconvolution of the magnetometer output was developed in order to obtain more detailed variations of the magnetization than permitted by the spatial resolution of the pickup coil (approximately 11 cm). The magnetization vector was modeled as a smoothly changing sequence parametrized by L_2 norm of second-order difference and then deconvolved using a matrix calculation as a smoothness constrained least squares method. The optimum smoothness was obtained by minimizing Akaike's Bayesian Information Criterion which is a measure of the logarithm of the likelihood. This deconvolution scheme was applied to pass-through data artificially produced by convolving synthetic reversal record and adding a Gaussian noise. The amplitude of the noise was estimated and the variations shorter than the spatial resolution of the sensor were obtained. The deconvolution also was applied to the real pass-through data from Holes 769A and 769B measured at intervals of 5 mm. The deconvolution revealed variations of the magnetizations with a maximum spatial resolution of about 2 cm. The magnetizations after deconvolution were in good agreement with magnetization values measured separately on cube samples taken at intervals of 5 or 10 cm.

Introduction

The Ocean Drilling Program (ODP) has long been using a pass-through cryogenic magnetometer as one of the routine measurements on 1.5-m-long samples at intervals of 10 cm. ODP's paleomagnetic data obtained for advanced piston cores (APC) on board the *Joides Resolution* are invaluable because on-site measurements prevent samples from alteration. Furthermore, the large cross section of obtainable samples (17.1 cm^2) results in an increase in the sensitivity of the measurements. Higher resolution pass-through measurements (e.g., at intervals of 5 mm) on the sediments of high sedimentation rates will provide more detailed records of secular variations, reversals, and excursions of geomagnetic field.

The signal detected by the sensor pick-up coils of the magnetometer at a certain position comes from magnetizations lying in the broad region of sensitivity of the pick-up coils. In order to obtain real remanent magnetization vectors of a long-core, the output of a pass-through magnetometer needs to be deconvolved. This type of deconvolution is achieved by an operation in the frequency domain which involves dividing the magnetometer output by the sensor response. As the sensor response function is typically a smooth bell-shaped curve and has low amplitude for higher frequency components, high-frequency noise in the output signal can easily be exaggerated. Reduction of high-frequency noise is necessary to obtain a meaningful solution of the magnetization.

The first attempt to deconvolve long-core paleomagnetic data was made by *Dodson et al.* [1974]. They measured the magnetic remanence of a core sample (length of 1 m) using a long-core cryogenic magnetometer and deconvolved the data by low-pass filtering in frequency space. The appropriate filter characteristics were determined subjectively by visual analysis of the displayed signal.

Constable and Parker [1991] developed an alternative deconvolution scheme using a smoothness-constrained least squares method for long-core paleomagnetic data. They assumed that the magnetization changes smoothly and expressed the data, the magnetization, and the sensor response in terms of cubic spline functions. The smoothness of the magnetization was measured by L_2 norm of second-order difference, and the degree of smoothness was chosen so that the fitting residual equals the observational error. These errors were estimated by the root-mean-square value of measurements corresponding to the region beyond the influence of the core

[1]Now at Marine Geology Department, Geological Survey of Japan, Tsukuba.

Paper number 95JB02811.
0148-0227/96/95JB-02811$05.00

magnetization. Although their deconvolution scheme has been quite successful for a well-defined noise level, it tends to be unstable when the noise level is underestimated [*Oda and Shibuya*, 1994].

We [*Oda and Shibuya*, 1994] recently developed ABIC (Akaike's Bayesian Information Criterion) minimizing deconvolution scheme for one component in the form of a smoothness-constrained least squares method. ABIC is a measure of the logarithm of the likelihood for a Bayes model, through which prior information of the model can be introduced objectively [*Akaike*, 1980]. By applying this scheme on the whole-core remanence data of a U-channel core measured at intervals of 5 mm, we have obtained magnetization consistent with the magnetization of thin sections measured separately on the same core.

ABIC minimization already has been applied successfully to several geophysical problems including tidal analysis (BAYTAP-G [*Tamura et al.*, 1991]), estimation of Bouguer reduction density [*Murata*, 1990], and the smoothing of paleomagnetic data [*Tsunakawa*, 1992]. Proper parametrization of the system, evaluation of minimum ABIC and analyses of the residuals provide objective information of the better Bayes modeling which allows one to obtain progressively improved solutions.

All the formerly developed deconvolutions were conducted on each magnetization vector component separately, although interactions between different components can in reality exist. During the pass-through measurement of ODP, the archive half samples are inserted in the lower half of the borehole of the magnetometer. This off-centered configuration produces cross terms between the x and z components of the magnetization. Thus the advanced form of ABIC minimizing deconvolution was developed in order to treat three vector components simultaneously and incorporate the cross terms. The newly developed three-dimensional deconvolution scheme was applied to the pass-through data of ODP Leg 124 measured at 5-mm intervals, and the synthesized data and results were investigated.

Formulation

Equation of Observation

Pass-through measurements on ODP's research vessel are conducted on the archive half of the core samples which were split from 1.5-m-long whole-core samples. During paleomagnetic measurements, the archive half cores passes through in the lower half of the borehole of the magnetometer (Figure 1a). Due to this configuration, the x component of magnetization appears in z axis pick-up coil and z component in x axis (Figure 1b). Thus the calculations are conducted in three-dimensional space in order to include cross terms.

In this work we assume that the magnetization is composed of uniformly magnetized thin slices of constant thickness. Consequently, it is possible to express the equation of observation in a discrete form utilizing a matrix equation which relates the magnetometer output, response function, and magnetization by

$$\mathbf{d} = \mathbf{R_0 m} + \mathbf{e}, \tag{1}$$

where $\mathbf{d}$ denotes the whole-core remanence data, $\mathbf{m}$ the magnetization of the sample, $\mathbf{R_0}$ a matrix whose columns are composed of the sensor responses, and $\mathbf{e}$ the noise in the whole-core data. Because the true response function $\mathbf{R_0}$ cannot be known practically, it is typically replaced by an empirical response term, $\mathbf{R}$, such that the error of the empirical response term can be expressed as $\delta\mathbf{R} = \mathbf{R} - \mathbf{R_0}$ [e.g., *Okamoto*, 1992]. Therefore (1) can be rewritten as

$$\mathbf{d} = (\mathbf{R} - \delta\mathbf{R})\mathbf{m} + \mathbf{e}, \tag{2a}$$

or

$$\mathbf{d} = \mathbf{R m} + \boldsymbol{\varepsilon}, \tag{2b}$$

where ε is an equivalent noise which equals $(-\delta\mathbf{R}\mathbf{m} + \mathbf{e})$. As a result, the error in the response function is included in ε. Consequently, one can write an empirical response equation expressed in terms of the x, y, and z components as

$$\begin{bmatrix} \mathbf{d_x} \\ \mathbf{d_y} \\ \mathbf{d_z} \end{bmatrix} = \begin{bmatrix} \mathbf{R_{xx}} & \mathbf{0} & \mathbf{R_{zx}} \\ \mathbf{0} & \mathbf{R_{yy}} & \mathbf{0} \\ \mathbf{R_{xz}} & \mathbf{0} & \mathbf{R_{zz}} \end{bmatrix} \begin{bmatrix} \mathbf{m_x} \\ \mathbf{m_y} \\ \mathbf{m_z} \end{bmatrix} + \begin{bmatrix} \boldsymbol{\varepsilon_x} \\ \boldsymbol{\varepsilon_y} \\ \boldsymbol{\varepsilon_z} \end{bmatrix}, \tag{3}$$

where the subscripts correspond to the vector component in that respective direction of orientation. $\mathbf{R_{ab}}$ is defined to be the ath component of magnetization to the b axis pick-up coil. Furthermore, each component of $\mathbf{d}$, $\mathbf{m}$, $\mathbf{R}$, and ε is expressed as

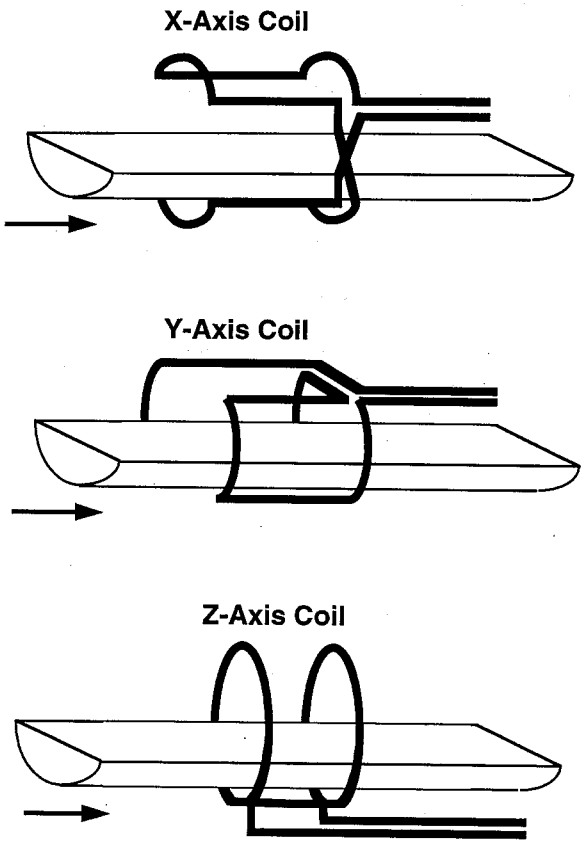

Figure 1a. Configurations of pick-up coils and archive half sample during pass-through measurement for x, y, and z axes.

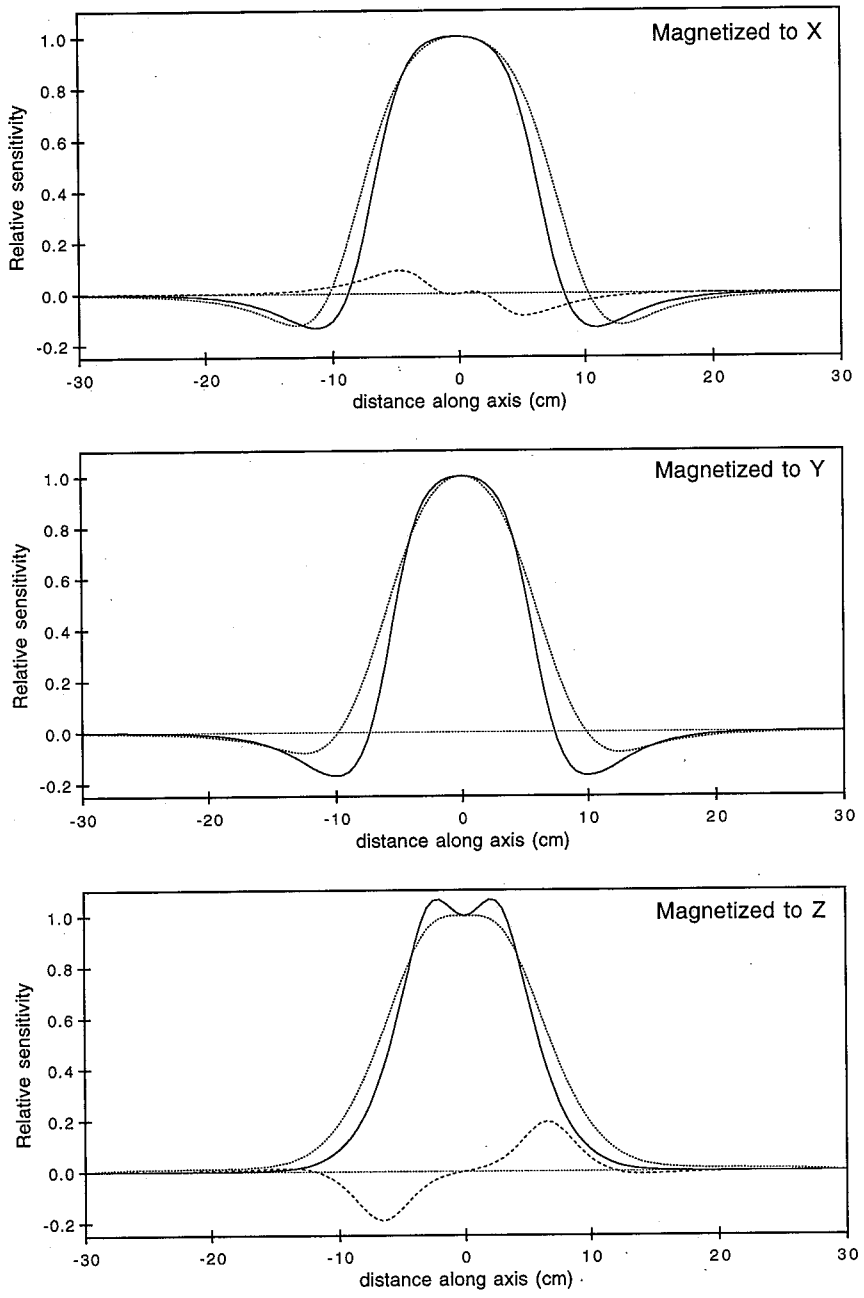

Figure 1b. Sensor response curves for each axis (solid lines) and cross terms (dashed lines) in x and z axes, compared with the old response measured at the center of the bore-hole (dotted lines).

$$\mathbf{d_b} = \begin{pmatrix} d_{b1} \\ d_{b2} \\ \vdots \\ d_{bN} \end{pmatrix} \quad \mathbf{m_a} = \begin{pmatrix} m_{a1} \\ m_{a2} \\ \vdots \\ m_{aM} \end{pmatrix} \quad \boldsymbol{\varepsilon_b} = \begin{pmatrix} \varepsilon_{b1} \\ \varepsilon_{b2} \\ \vdots \\ \varepsilon_{bN} \end{pmatrix}$$

$$\mathbf{R_{ab}} = \begin{pmatrix} R_{ab-l} & \cdots & R_{ab-r} & & 0 \\ \vdots & \ddots & & \ddots & \\ R_{ab0} & & \ddots & & R_{ab-r} \\ \vdots & \ddots & & \ddots & \vdots \\ R_{ab+l} & & \ddots & & R_{ab-l} \\ \vdots & \ddots & & \ddots & \vdots \\ R_{ab+r} & & \ddots & & R_{ab0} \\ & \ddots & & \ddots & \vdots \\ 0 & & R_{ab+r} & \cdots & R_{ab+l} \end{pmatrix}.$$

Here N is the total number of measured points, M is the number of unit slices of the sample, l is the number of measured points beyond the sample and r is half the number of measured points of the sensor response. R_{abc} is the response value measured at position c; R_{ab0}, R_{ab-r}, and R_{ab+r}, correspond to the response values at the center of the sensor, and left and right ends of the detection limit.

Bayesian Statistics

We assume that the noise in three axes are independent and can be expressed as a Gaussian noise of zero mean and variance, v. The likelihood function of the whole-core data is given by

$$L(\mathbf{d}|\mathbf{m},\nu)=\left(\frac{1}{2\pi\nu}\right)^{\frac{3N}{2}}\exp\left\{-\frac{1}{2\nu}\|\mathbf{d}-\mathbf{Rm}\|^2\right\}, \quad (4)$$

where $\|\mathbf{a}\|^2$ represents Euclidean norm of the vector $\mathbf{a}$.

In order to reduce the instability of the solution, the magnetization is assumed to change smoothly along the core. The smoothness of the magnetization can be measured by the L_2 norm of second-order difference as

$$\sum_{i=1}^{M}\left\{\left|m_{xi}-2m_{xi-1}+m_{xi-2}\right|^2+\left|m_{yi}-2m_{yi-1}+m_{yi-2}\right|^2+\left|m_{zi}-2m_{zi-1}+m_{zi-2}\right|^2\right\},$$

which can be presented simply by the matrix expression, $\|\mathbf{D}^*\mathbf{m}^*\|^2$, where $\mathbf{D}^*$ and $\mathbf{m}^*$ are defined as

$$\mathbf{D}^*=\begin{pmatrix}\mathbf{D}_1^* & \mathbf{0} & \mathbf{0}\\ \mathbf{0} & \mathbf{D}_1^* & \mathbf{0}\\ \mathbf{0} & \mathbf{0} & \mathbf{D}_1^*\end{pmatrix}, \qquad \mathbf{m}^*=\begin{pmatrix}m_{x-1}\\ m_{x0}\\ \mathbf{m_x}\\ m_{y-1}\\ m_{y0}\\ \mathbf{m_y}\\ m_{z-1}\\ m_{z0}\\ \mathbf{m_z}\end{pmatrix},$$

$$\mathbf{D}_1^*=\begin{pmatrix}1 & -2 & 1 & & \mathbf{0}\\ & \ddots & \ddots & \ddots & \\ \mathbf{0} & & 1 & -2 & 1\end{pmatrix}.$$

In this case $\mathbf{D}^*$ denotes a matrix of second-order difference composed of $\mathbf{D}_1^*$ which represents second-order differences for one component, while $\mathbf{m}^*$ is composed of a magnetization vector and six properly chosen parameters $m_{x\,-1}$, $m_{x\,0}$, $m_{y\,-1}$, $m_{y\,0}$, $m_{z\,-1}$, and $m_{z\,0}$. Again, by introducing the following $\mathbf{D}$ and $\mathbf{z}$

$$\mathbf{D}=\begin{pmatrix}\mathbf{D}_1 & \mathbf{0} & \mathbf{0}\\ \mathbf{0} & \mathbf{D}_1 & \mathbf{0}\\ \mathbf{0} & \mathbf{0} & \mathbf{D}_1\end{pmatrix}, \qquad \mathbf{z}=\begin{pmatrix}-m_{x-1}+2m_{x0}\\ -m_{x0}\\ 0\\ \vdots\\ 0\\ -m_{y-1}+2m_{y0}\\ -m_{y0}\\ 0\\ \vdots\\ 0\\ -m_{z-1}+2m_{z0}\\ -m_{z0}\\ 0\\ \vdots\\ 0\end{pmatrix},$$

$$\mathbf{D}_1=\begin{pmatrix}1 & & & & \\ -2 & 1 & & \mathbf{0} & \\ 1 & -2 & 1 & & \\ & \ddots & \ddots & \ddots & \\ \mathbf{0} & & 1 & -2 & 1\end{pmatrix},$$

the second-order difference $\|\mathbf{D}^*\mathbf{m}^*\|^2$ can be transformed to $\|\mathbf{z}-\mathbf{Dm}\|^2$, and henceforth the newly introduced six parameters can be isolated in vector $\mathbf{z}$. In order to express the changing magnetizations smoothly, the second-order difference is assumed to distribute as a Gaussian with zero mean and variance ν/u^2. By using the matrix expression above, the prior distribution of magnetization $\mathbf{m}$ is given by

$$p(\mathbf{m}|\nu,u)=\alpha\left(\frac{u^2}{2\pi\nu}\right)^{\frac{3M}{2}}|\mathbf{D}^t\mathbf{D}|^{\frac{1}{2}}\exp\left\{-\frac{u^2}{2\nu}\|\mathbf{z}-\mathbf{Dm}\|^2\right\}, \quad (5)$$

where u is a hyperparameter that express the degree of smoothness, α is a normalization constant, and $|\mathbf{A}|$ represents the determinant of the matrix $\mathbf{A}$.

According to the Bayes' theorem [e.g., *Akaike*, 1989], the posterior distribution of the magnetization is constituted by the likelihood function and the prior distribution as

$$p_{\text{post}}(\mathbf{m}|\mathbf{d},\nu,u)\propto L(\mathbf{d}|\mathbf{m},\nu)\cdot p(\mathbf{m}|\nu,u), \quad (6a)$$

so that

$$p_{\text{post}}(\mathbf{m}|\mathbf{d},\nu,u)=\left(\frac{1}{2\pi\nu}\right)^{\frac{3N}{2}}\left(\frac{u^2}{2\pi\nu}\right)^{\frac{3M}{2}}|\mathbf{D}^t\mathbf{D}|^{\frac{1}{2}}\exp\left(-\frac{S}{2\nu}\right), \quad (6b)$$

where S is the formula

$$S=\|\mathbf{d}-\mathbf{Rm}\|^2+u^2\|\mathbf{z}-\mathbf{Dm}\|^2. \quad (7)$$

For given $\mathbf{d}$, ν, and u the maximum likelihood distribution of $\mathbf{m}$ can be obtained by minimizing S. This minimization can be interpreted as a constrained least squares method which is generally used for solving inverse problems [e.g., *Tarantola*, 1987; *Dimri*, 1992].

Akaike's Bayesian Information Criterion

Akaike's Bayesian Information Criterion was proposed by *Akaike* [1980] to determine the optimum hyperparameter for a Bayes model. The optimum hyper parameter can be calculated by minimizing ABIC, which is given by a log maximum marginal likelihood as

$$\text{ABIC}=-2\log\int p_{\text{post}}(\mathbf{m}|\mathbf{d},\nu,u)d\mathbf{m}+2(\text{number of adjusted hyperparameters}) \quad (8)$$

By substituting (6b) into (8), ABIC for the deconvolution becomes

$$\text{ABIC}=3N\log(2\pi\nu)-3M\log(u^2)-\log|\mathbf{D}^t\mathbf{D}|^{\frac{1}{2}}-2\log\int\left(\frac{1}{2\pi\nu}\right)^{\frac{3M}{2}}\exp\left(-\frac{S}{2\nu}\right)d\mathbf{m}+2. \quad (9)$$

Furthermore, (7) can be transformed by using the following definitions

$$\mathbf{b}=\begin{bmatrix}\mathbf{d}\\ u\mathbf{z}\end{bmatrix}, \qquad \mathbf{F}=\begin{bmatrix}\mathbf{R}\\ u\mathbf{D}\end{bmatrix},$$

so that S becomes

$$S=\|\mathbf{b}-\mathbf{Fm}\|^2. \quad (10)$$

By defining $\mathbf{m_0}$ to be the value of $\mathbf{m}$ which minimizes S, the best solution, $\mathbf{Fm_0}$, is closer to $\mathbf{b}$ than any other vector $\mathbf{Fm}$. Therefore S can be decomposed to $\|\mathbf{b}-\mathbf{Fm_0}\|^2$ and $\|\mathbf{F}(\mathbf{m}-\mathbf{m_0})\|^2$ as

$$S=\|\mathbf{b}-\mathbf{Fm_0}\|^2+\|\mathbf{F}(\mathbf{m}-\mathbf{m_0})\|^2, \quad (11a)$$

and thus

$$S=S^*+\|\mathbf{F}(\mathbf{m}-\mathbf{m_0})\|^2, \quad (11b)$$

where

$$S^* = \|\mathbf{d} - \mathbf{R}\mathbf{m}_0\|^2 + u^2\|\mathbf{z} - \mathbf{D}\mathbf{m}_0\|^2. \quad (12)$$

The integral term in (9) can be calculated by substituting (10) and (11b) successively which leads to

$$-2\log\int\left(\frac{1}{2\pi v}\right)^{\frac{3M}{2}}\exp\left(-\frac{S}{2v}\right)d\mathbf{m} = \frac{S^*}{v}$$

$$-2\log\int\left(\frac{1}{2\pi v}\right)^{\frac{3M}{2}}\exp\left(-\frac{1}{2v}\|\mathbf{F}(\mathbf{m}-\mathbf{m}_0)\|^2\right)d\mathbf{m}, \quad (13a)$$

and thus

$$-2\log\int\left(\frac{1}{2\pi v}\right)^{\frac{3M}{2}}\exp\left(-\frac{S}{2v}\right)d\mathbf{m} = \frac{S^*}{v} + \log|\mathbf{F}^t\mathbf{F}|. \quad (13b)$$

By substituting (13b) into (9), one obtains the following relationship

$$\mathrm{ABIC} = 3N\log\left(\frac{2\pi S^*}{3N}\right) + 3N - 3M\log(u^2) - \log|\mathbf{D}^t\mathbf{D}| + \log|\mathbf{F}^t\mathbf{F}| + 2. \quad (14)$$

By differentiating with respect to v, one can determine the value of v which minimizes ABIC as $v_{\min} = S^*/3N$. The final form of ABIC is then obtained by substituting $v_{\min}$ into (13b) so that

$$\mathrm{ABIC} = 3N\log\left(\frac{2\pi S^*}{3N}\right) + 3N - 3M\log(u^2) - \log|\mathbf{D}^t\mathbf{D}| + \log|\mathbf{F}^t\mathbf{F}| + 2. \quad (15)$$

Minimum ABIC is searched in ln u space by initially bracketing by Golden Section Search and subsequently converging by Brent's Method to a tolerance of 0.1, which is sufficient to achieve convergence in this case [*Press et al.*, 1992].

Matrix Calculation

We can obtain minimum S^* in (15) and $\mathbf{m}_0$ in (14) by basic matrix calculations. The parameters in $\mathbf{z}$ are included in $\mathbf{m}^*$ in combination with $\mathbf{m}$ and can be minimized simultaneously. The modified formula is given as

$$\|\mathbf{d} - \mathbf{R}\mathbf{m}_0\|^2 + u^2\|\mathbf{z} - \mathbf{D}\mathbf{m}_0\|^2 = \|\mathbf{b} - \mathbf{F}\mathbf{m}_0\|^2, \quad (16a)$$

$$\left\|\mathbf{d} - \mathbf{R}\mathbf{m}_0\right\|^2 + u^2\|\mathbf{z} - \mathbf{D}\mathbf{m}_0\|^2 = \left\|\mathbf{b}^* - \mathbf{F}^*\mathbf{m}_0^*\right\|^2, \quad (16b)$$

where

$$\mathbf{b}^* = \begin{bmatrix}\mathbf{d}\\0\\\vdots\\0\end{bmatrix},\quad \mathbf{F}^* = \begin{bmatrix}\mathbf{R}^*\\u\mathbf{D}^*\end{bmatrix}$$

$$\mathbf{R}^* = \begin{bmatrix}\mathbf{R}^*_{xx} & \mathbf{0} & \mathbf{R}^*_{zx}\\ \mathbf{0} & \mathbf{R}^*_{yy} & \mathbf{0}\\ \mathbf{R}^*_{xz} & \mathbf{0} & \mathbf{R}^*_{zz}\end{bmatrix},\quad \mathbf{R}^*_{ab} = \begin{bmatrix}0 & 0\\ \vdots & \vdots\\ 0 & 0\end{bmatrix}\ \mathbf{R}_{ab}$$

Minimization of $\|\mathbf{b}^* - \mathbf{F}^*\mathbf{m}_0^*\|^2$ can be accomplished by solving $\mathbf{F}^{*t}\mathbf{b} = \mathbf{F}^{*t}\mathbf{F}^*\mathbf{m}_0^*$. Given $\mathbf{G} = \mathbf{F}^{*t}\mathbf{F}^*$, magnetization can be obtained by the following expression

$$\mathbf{m}_0^* = \mathbf{G}^{-1}\mathbf{F}^{*t}\mathbf{b}^*. \quad (17)$$

Furthermore, $\mathbf{G}^{-1}$ can be calculated by LDU (Lower triangular, Diagonal, and Upper triangular matrixes) decomposition using the Modified Cholesky Method [*Togawa*, 1971] with $\mathbf{m}_0^*$ obtained by (16b).

Error and Resolution

It can be shown that the magnetization distributes as a Gaussian according to the covariance matrix $\varepsilon^2\mathbf{G}^{-1}$. Let g_{ii} be the ith diagonal component of $\mathbf{G}^{-1}$, the estimated error of magnetization for ith slice can then be expressed by

$$\sigma_{mi} = \varepsilon\sqrt{g_{ii}}, \quad (18)$$

where ε is the standard deviation of magnetometer output, which can be estimated from the residual of model and measurement. In the case of 95% confidence level for magnetization, σ_{mi} must be multiplied by a factor of 1.96. The

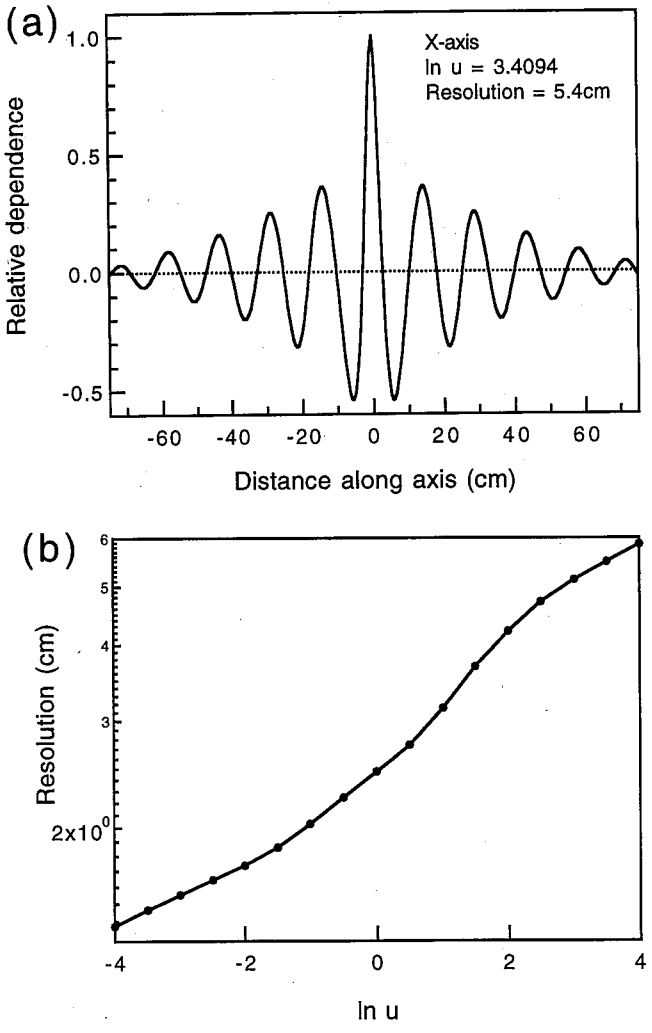

Figure 2. (a) Kernel for the x axis response function at ln u = 3.4. The spatial resolution measured by zero crossings of the curve is 5.4 cm. (b) Plot of resolution versus ln u measured by zero crossings of the kernel.

nondiagonal component of the covariance matrix represents the degree of which a given measurement is dependent on the neighboring data points. Typical matrix components corresponding to the x axis are given in Figure 2a. The resolution of the data points can be defined as the width of zero crossing points. The resolution at the center of the core for x, y and z axes were calculated and the average value was defined to be the resolution for the data. For a given response matrix and core length, resolution can be accurately calculated as a function of ln u (Figure 2b).

Applications

Description of Measurement System

Immediately after drilling, the 9.5-m-long APC samples are cut into 1.5-m-long sections. These whole-round core sections are then sent to the multisensor track and are subsequently split into working and archive halves. The archive halves are measured by using a pass-through type SQUID (Superconducting Quantum Interference Device) rock magnetometer (model 760R, 2G Enterprises) on board the *Joides Resolution*. Samples are inserted into the borehole of the magnetometer by a plastic boat connected to a stepping motor with a polyurethane rope. The samples are demagnetized several times with an AF demagnetizer (model 2G600, 2G Enterprises) in three axes in line with the cryogenic SQUID rock magnetometer (SRM). A multiserial communication board installed in the PC-AT compatible computer controls the SRM, the demagnetizer, and the stepping motor that transports the core samples. The SQUID electronics of the SRM are operated at the 1x scale using a flux-counting mode. The x axis component of the SQUID magnetometer must be inverted to get the vector components in the sample frame (Core-north, Core-east, Down-core).

Sensor response curves were obtained by measurements on thin half-circle-shaped standard samples made of magnetic tape magnetized to the specific axes. Measurements were conducted twice for each axis and were averaged to obtain sensor response curves (Figure 1b). Note that the magnetization in x axis is detected by z axis pick-up coil with peak amplitude of about 10% of x axis amplitude and magnetization in z axis appear in x axis coil as 20% of x axis.

Synthetic Data

In order to test the deconvolution scheme, synthetic magnetization was produced according to the following equation,

$$x_i = 0$$

$$y_i = 1\times10^{-6}\left[\frac{i-150}{150} + 0.05\sin\left(\frac{2\pi i}{10}\right)\right] \qquad (19)$$

$$z_i = 1\times10^{-6}\left[0.3\left(\frac{i-150}{150}\right) + 0.1\sin\left(\frac{2\pi i}{40}\right)\right]$$

where i is an index of the data points. The measurement spacing was set to 5 mm and the length of the core was 150 cm. An additional 15 cm on both sides of the core was also included in the measurement. In order to mimic the geomagnetic reversal records, the y and z components of the data were designed to change polarity near the middle of the synthetic long-core data with overlapping sinusoidal fluctuations of two wavelengths (5 cm in y axis and 20 cm in z axis), while x was maintained at null in order to observe the cross terms produced by the z component magnetization. After convolving the magnetization by the sensor response curve, Gaussian noise was added with the amplitude corresponding to S/N ratios of 51.6.

ABIC draws a simple downward convex curve versus ln u which obtains a minimum of -26188 at ln u = 3.41 (Figure 3). The results of deconvolution are shown on Figure 4. The variation of shorter wavelength in the y axis (2.5 cm in half wavelength) were smeared out by the noise and therefore could not be detected by deconvolution since the spatial resolution is 5.4 cm for ln u = 3.41 (Figure 2b). On the contrary, longer wavelength fluctuation in z axis (10 cm in half wavelength) are recovered by deconvolution. Although this z axis fluctuation can be seen before deconvolution, the fluctuation is more pronounced and has a larger amplitude following deconvolution. This fluctuation in z axis (dots) is in good agreement with the original one (dashed line). The x component suffers only small variation from the expected result and can be considered accurate.

The residual for all the components are distributed as a Gaussian without any systematic change. The estimated S/N ratio for this case is 52.7, which is very close to the value of the original data (51.6). These characteristics of noise are consistent with the primary assumption that the noise distribution is Gaussian.

Real Data

Deep sea sediment cores from ODP Leg 124 were used as examples of real pass-through data. High sedimentation rates and high concentration of magnetic mineral of these cores provided materials suitable for detailed magnetostratigraphic study [*Rangin et al.*, 1990]. Four sections from Site 769 which correspond to the Brunhes/Matuyama polarity transition were used, including 769B-7H6 (1.5 m long), 769B-7H7 (0.7 m long), 769A-7H4 (1.5 m long) and 769A-7H5 (1.5 m long). These samples were measured by a pass-through cryogenic

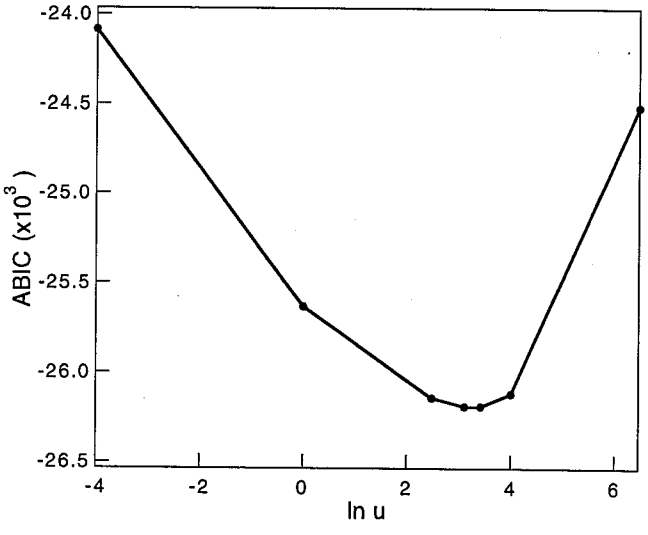

Figure 3. ABIC values are plotted versus ln u values for the deconvolution of synthetic data with Gaussian noise of S/N= 51.6. ABIC comes to minimum value of -26188 where ln u equals 3.41 around the middle of a downward convex curve.

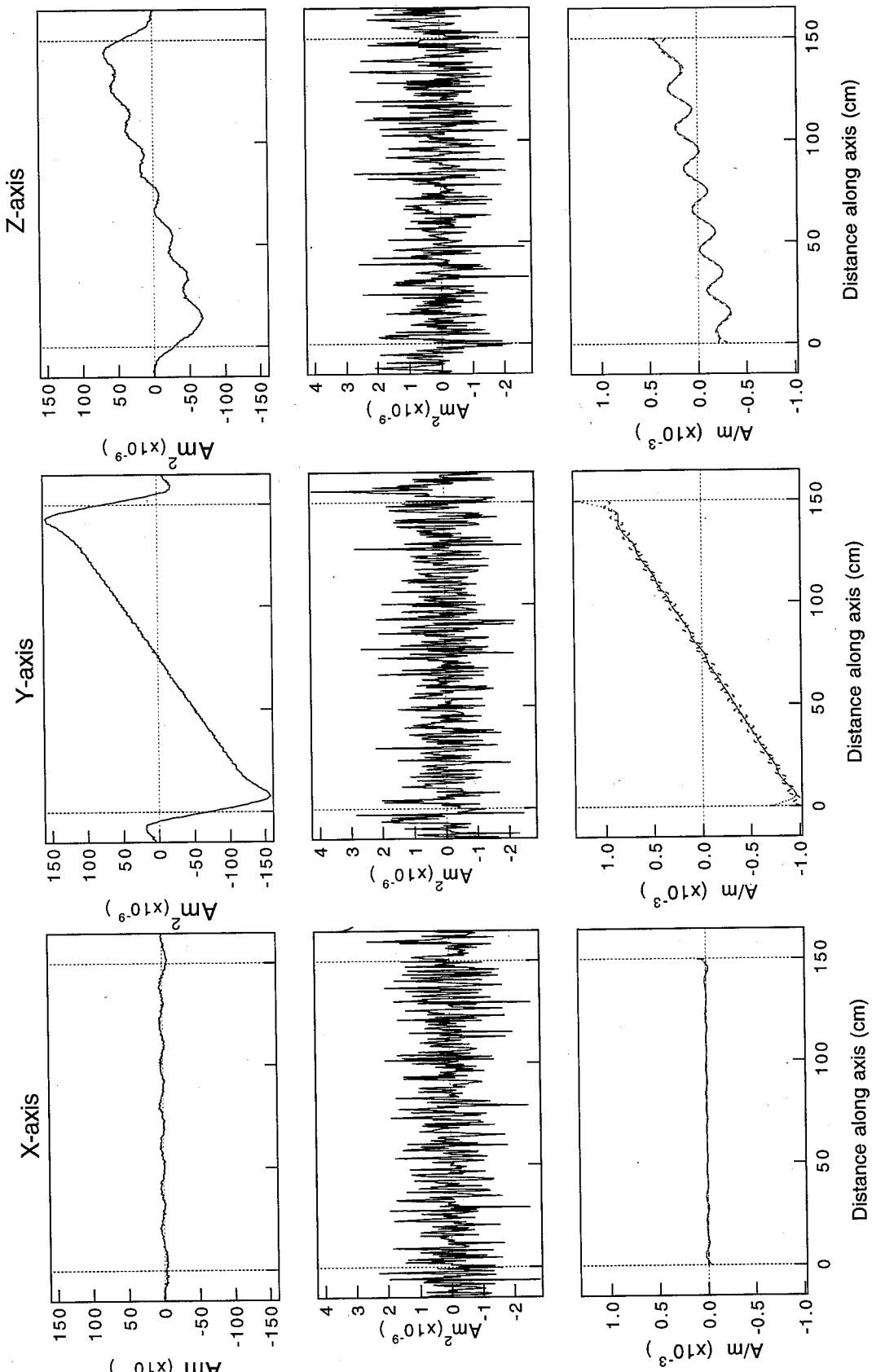

Figure 4. Results of deconvolution for the synthetic magnetization record with polarity reversal and fluctuations in y and z axes. Results for x, y, and z axes are shown from left to right columns. (Top) Magnetic moment artificially produced from the synthetic magnetization record by convolution and superposition of Gaussian noise with a S/N ratio of 51.6. (Middle) Residual of the original magnetic moment and the magnetic moment for model magnetization after deconvolution. (Bottom) Original synthetic magnetization before convolution (dashed lines) and the model magnetization obtained by deconvolution (dotted line).

magnetometer at intervals of 5 mm after exposure to alternating magnetic fields of 15 and 20 mT, including supplementary regions (15 cm) beyond the cores on both sides.

Prior to deconvolution, these data require three kinds of corrections (Figure 5). One correction involves the drift of the SQUID magnetometer, which can be treated by subtracting the baseline value on the PC-AT computer automatically following the acquisition of the SQUID output signal. After the drift correction, spike noises and stepwise jumps were recognized in the data as discontinuous points by monitoring magnetization and its derivative simultaneously on display. The presence of other electronic devices near the magnetometers may lead to noise such as spike noises. These errors can be eliminated by replacing the abnormal value with the average value of adjacent points.

Furthermore, abrupt stepwise jumps were recognized in the data. Some of them may be due to a miscounting of flux jumps, which correspond exactly to the magnetic moment of a flux quanta (ϕ_0) for the x, y, and z axes (1.740×10^{-4} emu/ϕ_0, 1.646×10^{-4} emu/ϕ_0, and 1.215×10^{-4} emu/ϕ_0). These were corrected easily by adding or subtracting the values corresponding to the flux quanta. However, other sources of jumps are recognized with values around $1\text{-}6 \times 10^{-5}$ emu, which are smaller than flux jump-related miscounting. In these cases unknown jumps in y axis are the most frequent noises, which occasionally appear at the same position in different demagnetization levels. The two kinds of jumps mentioned above result in an apparent drift due to the automatic drift correction (Figure 5a) and lead to overcorrection (Figure 5b). Therefore once jumps were removed (Figure 5c), the apparent drift should be subtracted from the data (Figure 5d).

The results of ABIC minimizing deconvolution on Section 124-769B-7H6 are shown in Figure 6. The magnetic moment measured with a pass-through magnetometer, residuals of calculated model moment, and the magnetization obtained by the deconvolution are given collectively for each axis. The minimum value for ABIC (-23465) occurs when ln u equals -2.09 (Table 1, trial a). Signal-to-noise (S/N) ratio for total magnetic moment is calculated as 566 by dividing the root-mean-square of the SQUID output by the root-mean-square of the residual. As a result, the deconvolution improved spatial resolution of magnetization to a maximum of 2 cm. Residuals are composed of white noise and periodic waves whose wavelength is about 15 cm. As the presence of periodic waves in the residuals contradict the assumption that the noise distribute as a Gaussian, the reason will be discussed later.

Deconvolution by the sensor response curves customarily used on ODP, measured in the borehole center on the standard sample (Figure 1b, dotted lines), was also conducted and the results were compared with those of the new response curves (Figure 7). The minimum ABIC value is much higher (-20723) than that for the correct response (-23465), suggesting that the sensor response is greatly improved (compare trials a and b, Table 1). Additionally, the estimated S/N ratio was also lowered from 566 to 123 by using the old responses.

The response curve without cross terms was also used for the deconvolution (Table 1, trial c). The results show higher minimum ABIC (-23015) and lower S/N ratio (482), which indicate that the cross terms improve the deconvolution. However, the difference in solution is not significant (Figure 8).

Our deconvolution scheme for single component [*Oda and Shibuya*, 1994] was also conducted separately in each axis (Table 1, trials d, e, and f) by using the new sensor response curves without cross terms. Minimum ABIC corresponding to one component of one data point (later referred to as "average ABIC") was also calculated for general comparison. The results are nearly the same as the new three-dimensional deconvolution (Figure 9) except that average ABIC (-21.41) is larger than that of trial a (-21.73). S/N ratio averaged for the three axes was 479, which is lower than the value for trial a .

Average values for trials d, e, and f were calculated as trial g in Table 1. The difference between trials c and g is smaller than between trials a and g, because both are deconvolved without cross terms. The most significant difference recognized for these tests was between trials a and b, suggesting that the old response curves formerly used on *Joides Resolution* should more appropriately be replaced by the new response curves.

Connect Adjacent Sections

In order to deconvolve two adjacent sections without breaks in magnetization, we have to deconvolve these two sections simultaneously. Two methods for linking adjacent sections into successive sequence were considered and tested. One method involved the overlap of data points from two data sets to produce a single set which was then deconvolved using the same equations as before though this new set now has a length twice that of either single section. Thirty data points at the end of the upper section and those at the beginning of the lower section, which were measured outside the sections, were overlapped by simply adding each point values. The average ABIC in this case is calculated as -21.73 and S/N ratio is 552 (Table 1, trial k). The results are shown on Figure 10 (dashed lines) for comparison with the results of separate deconvolution (dotted lines).

A second method of linking two adjoining sections deals with the magnetizations as a smoothly changing sequence leaving two data sets separate, which is achieved by replacing the vectors $\mathbf{d}$ and $\mathbf{m}$, and the matrixes $\mathbf{R}^*_{ab}$ and $\mathbf{D}^*_1$ with

$$\tilde{\mathbf{d}} = \begin{bmatrix} \mathbf{d_{1x}} \\ \mathbf{d_{2x}} \\ \mathbf{d_{1y}} \\ \mathbf{d_{2y}} \\ \mathbf{d_{1z}} \\ \mathbf{d_{2z}} \end{bmatrix}, \quad \tilde{\mathbf{m}} = \begin{bmatrix} m_{x-1} \\ m_{x0} \\ \mathbf{m_{1x}} \\ \mathbf{m_{2x}} \\ m_{y-1} \\ m_{y0} \\ \mathbf{m_{1y}} \\ \mathbf{m_{2y}} \\ m_{z-1} \\ m_{z0} \\ \mathbf{m_{1z}} \\ \mathbf{m_{2z}} \end{bmatrix}, \quad \tilde{\mathbf{R}}^*_{ab} = \begin{bmatrix} 0 & 0 & & \\ \vdots & \vdots & \mathbf{R^*_{1ab}} & \mathbf{0} \\ 0 & 0 & & \\ 0 & 0 & & \\ \vdots & \vdots & \mathbf{0} & \mathbf{R^*_{2ab}} \\ 0 & 0 & & \end{bmatrix},$$

$$\tilde{\mathbf{D}}^*_1 = \mathbf{D}^*_1(N_1+N_2, M_1+M_2+2),$$

where each subscript 1 or 2 on vectors and matrixes correspond to first and second sections. Here matrix $\mathbf{R}^*$ is composed of $\mathbf{R}^*_1$ and $\mathbf{R}^*_2$, and two data sets $\mathbf{d}_1$ and $\mathbf{d}_2$ are dealt with separately, whereas matrix $\mathbf{D}^*_1$ is continuous along with diagonal component, such that the magnetization is considered as continuous between the two adjoining sections.

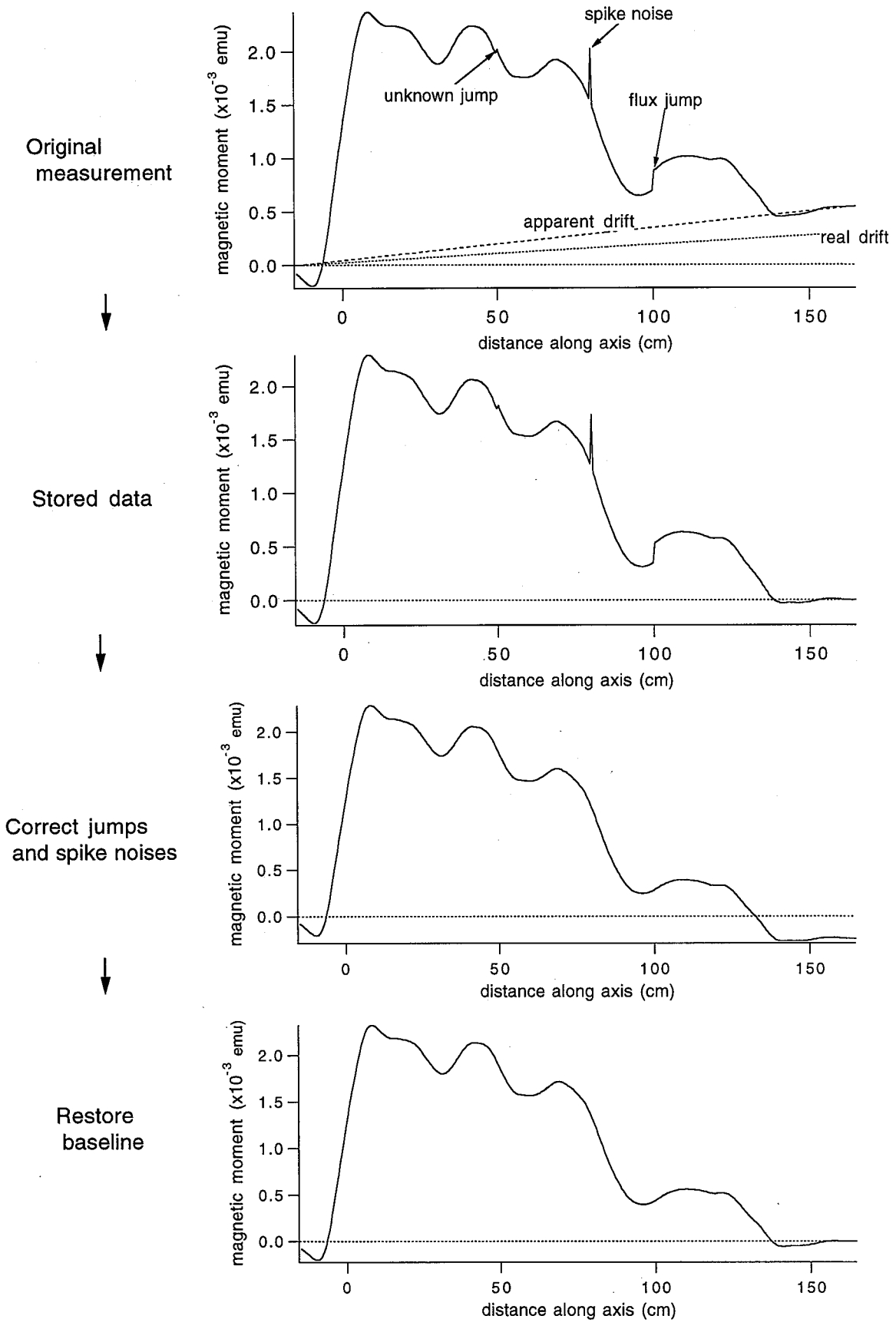

Figure 5. Diagram showing data correction procedures. (a) Row data directly acquired by PC-AT computer contains real drift of the magnetometer and apparent drift caused by jumps. (b) The difference between baseline value before and after the measurement is considered as drift and linearly interpolated values are stored in the file. (c) The corrections of jumps and spike noises result in overcorrection due to apparent drift, and (d) the baseline should be resumed by linear interpolation.

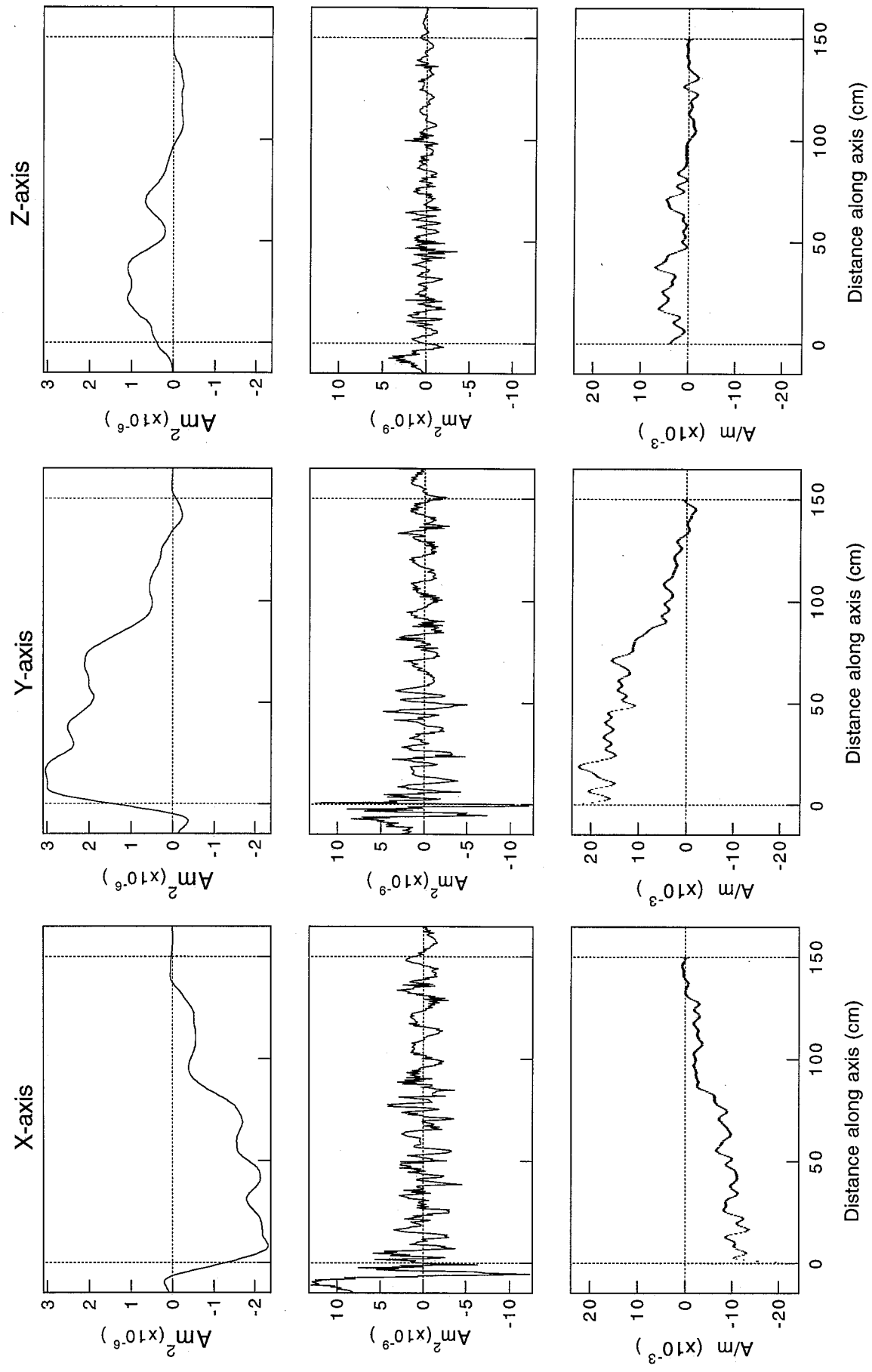

Figure 6. Results of deconvolution for the pass-through data of 769B-7H6 after demagnetization at peak alternating field of 20 mT (trial a). Results for x, y, and z axes are shown from left to right. (Top) Magnetic moment measured by the cryogenic magnetometer on board. (Middle) Residual of the original magnetic moment and the magnetic moment for model magnetization after deconvolution. (Bottom) Model magnetization obtained by deconvolution (dots with vertical bars representing 95% confidence limits).

Table 1. Results of Deconvolution for Different Measurements in Different Conditions

Trial	Demagnetization level, mT	Section	Response curve	Conditions	Number of Data	Number of Axes	ln u	Minimum ABIC	Average ABIC	S/N Ratio
a	20	769B-7H6	new	-	360	3	-0.209	-23465	-21.73	566
b	20	769B-7H6	old	-	360	3	1.386	-20728	-19.19	123
c	20	769B-7H6	new without X terms	-	360	3	-0.472	-23015	-21.31	482
d	20	769B-7H6	new without X terms	x axis	360	1	0.498	-7831	-21.75	535
e	20	769B-7H6	new without X terms	y axis	360	1	-0.239	-7794	-21.65	728
f	20	769B-7H6	new without X terms	z axis	360	1	-1.059	-7501	-20.84	175
g	20	769B-7H6	new without X terms	average (x, y, z)	360	1	-	-	-21.41	479
h	20	769B-7H7	new	-	200	3	-0.282	-13344	-22.24	401
i	20	769B-7H6, 7	new	average (7H6, 7)	560	3	-	-	-21.91	507
j	20	769B-7H6, 7	new	not overlapped	560	3	-0.402	-36732	-21.86	529
k	20	769B-7H6, 7	new	overlapped	500	3	-0.261	-32592	-21.73	552
l	20	769A-7H4	new	-	360	3	-0.281	-23173	-21.46	667
m	20	769A-7H5	new	-	360	3	-0.592	-24618	-22.79	547
n	20	769A-7H4, 5	new	average (7H4, 5)	720	3	-	-	-22.13	607
o	20	769A-7H4, 5	new	not overlapped	720	3	-0.496	-47220	-21.86	646
p	20	769A-7H4, 5	new	overlapped	660	3	-0.431	-43242	-21.84	702
q	15	769B-7H6	new	-	360	3	-0.403	-23409	-21.67	588

Average ABIC values were calculated by dividing the minimum ABIC values by the number of data and number of axes to compare the results in different conditions. This value corresponds to the minimum ABIC for one data point.

N_1 (N_2) is the number of measured points for the first (second) section, and M_1 (M_2) is the number of unit slices for the first (second) section. The average ABIC after deconvolution following the above equation is -21.86 and the S/N ratio is 529 (Table 1, trial j). The average ABIC values separately obtained for 769B-7H6 (Table 1, trial a) and 769B-7H7 (Table 1, trial h) were averaged (Table 1, trial i) as -21.91 and the average S/N ratio is 507. Among these three trials i, j, and k, the average ABIC is lowest for trial i and highest for trial k with minor differences, and likewise the S/N ratio is highest for trial k and lowest for trial i. The results of deconvolution by the second method are also shown for comparison in Figure 10 (solid lines). The difference between trials i and j is very small except within about 5 cm of both sides of the junction at 150 cm. However, the results of trial k (dashed lines) is dissimilar to both cases from 120 cm to 155 cm. Thus the method of connection without overlapping (trial j) is considered to be properly smoothed by assuming the continuous magnetization across the section boundary and was employed.

The results of deconvolution for Hole 769B are compared with the magnetization of cube samples (2.1 cm x 2.1 cm x 1.4 cm) taken from the working halves measured after demagnetization (Figure 11a). The cube samples taken at intervals of 5 cm were alternately subjected to either AF demagnetization or thermal demagnetization. The magnetizations after 20 mT for AF demagnetization and 400 °C for thermal demagnetization were used. Although both the size of the sample and measurement spacing are not sufficiently dense for quantitative comparison, these two results seem to be in favorable agreement. The magnetization intensity for cube samples is lower than those for pass-through measurement, perhaps as a result of drying-out of the samples.

The deconvolution was also conducted on samples from Hole 769A as trials n, o, and p (Table 1). The results show nearly the same tendency as those of Hole 769B (trials i, j, and k); that is, the average ABIC is minimum for separate deconvolution (trial n) and maximum for overlapped case (trial p), and S/N ratios are inverse. The result of deconvolution (trial p) was compared in Figure 11b with the magnetic remanence data of cube samples after 20 mT AF demagnetization measured at intervals of about 10 cm by *Schneider et al.* [1992]. Following deconvolution, the magnetizations of the pass-through data are in more favorable agreement with that of the cube samples than those for the pass-through data prior to deconvolution.

Discussions

Stability and Reliability of Deconvolution

The deconvolution scheme developed here was investigated in detail under various conditions utilizing real data. The correct response (Table 1, trial a) gave a lower ABIC value than any other incorrect response curves. This is quite consistent with the principle of maximum likelihood and confirms that the correct sensor response curve is the best estimate. Although ABIC is larger, the deconvolution without cross terms of the response curve is not significantly different from that of the correct response. This may confirm the stability of the deconvolution with respect to the response curve.

The noise estimated for the synthetic pass-through data is consistent with the noise superimposed before deconvolution. This may ensure that the deconvolution scheme is properly constructed when the noise can be well modeled by a Gaussian.

Comparison of the magnetizations after deconvolution with the direct measurement of cube samples for Holes 769A and 769B revealed considerable agreement in each case (Figure 11). Although the direct measurements were made only at intervals of 5 cm, certain trends are nonetheless noted. The

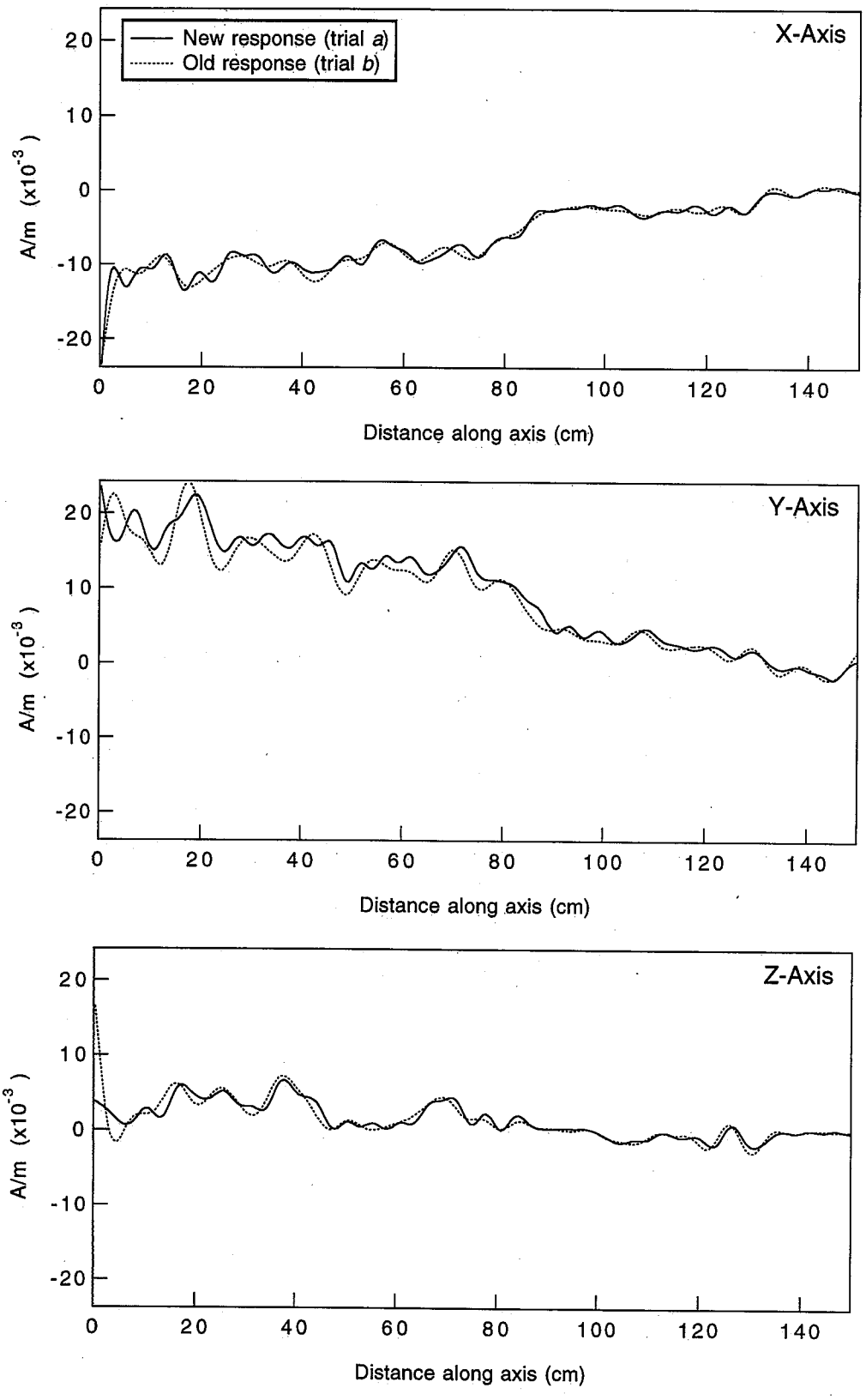

Figure 7. The magnetizations obtained by deconvolution for the measurements of Section 769B-7H6 at 20 mT AF demagnetization are plotted for the correct response curve (solid lines, trial a) and for the old response curve used conventionally on ODP's research vessel (dashed lines, trial b).

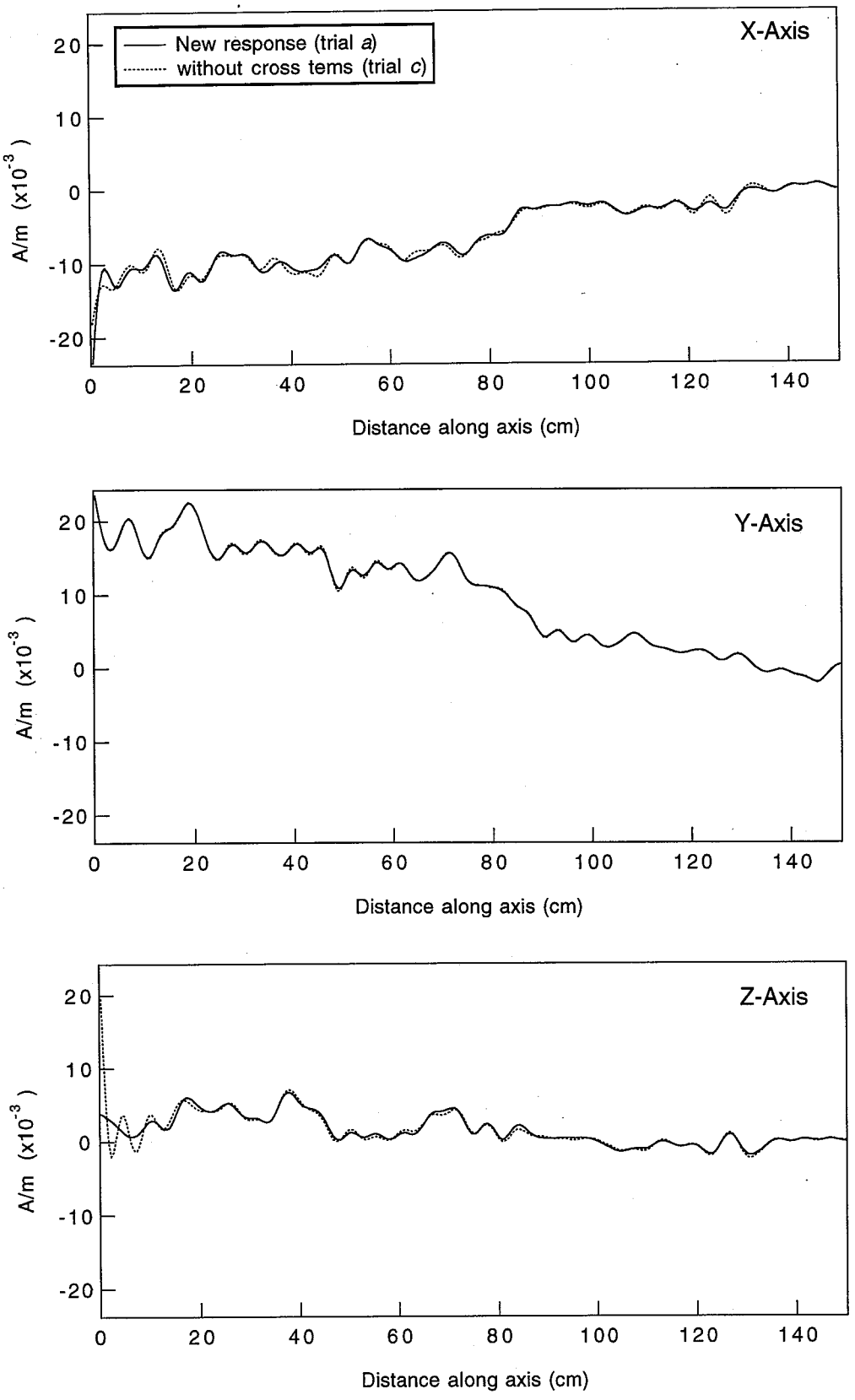

Figure 8. The magnetizations obtained by deconvolution for the measurements of Section 769B-7H6 at 20 mT AF demagnetization are plotted for the correct response curve (solid lines, trial a) and for the response without cross terms (dotted lines, trial c).

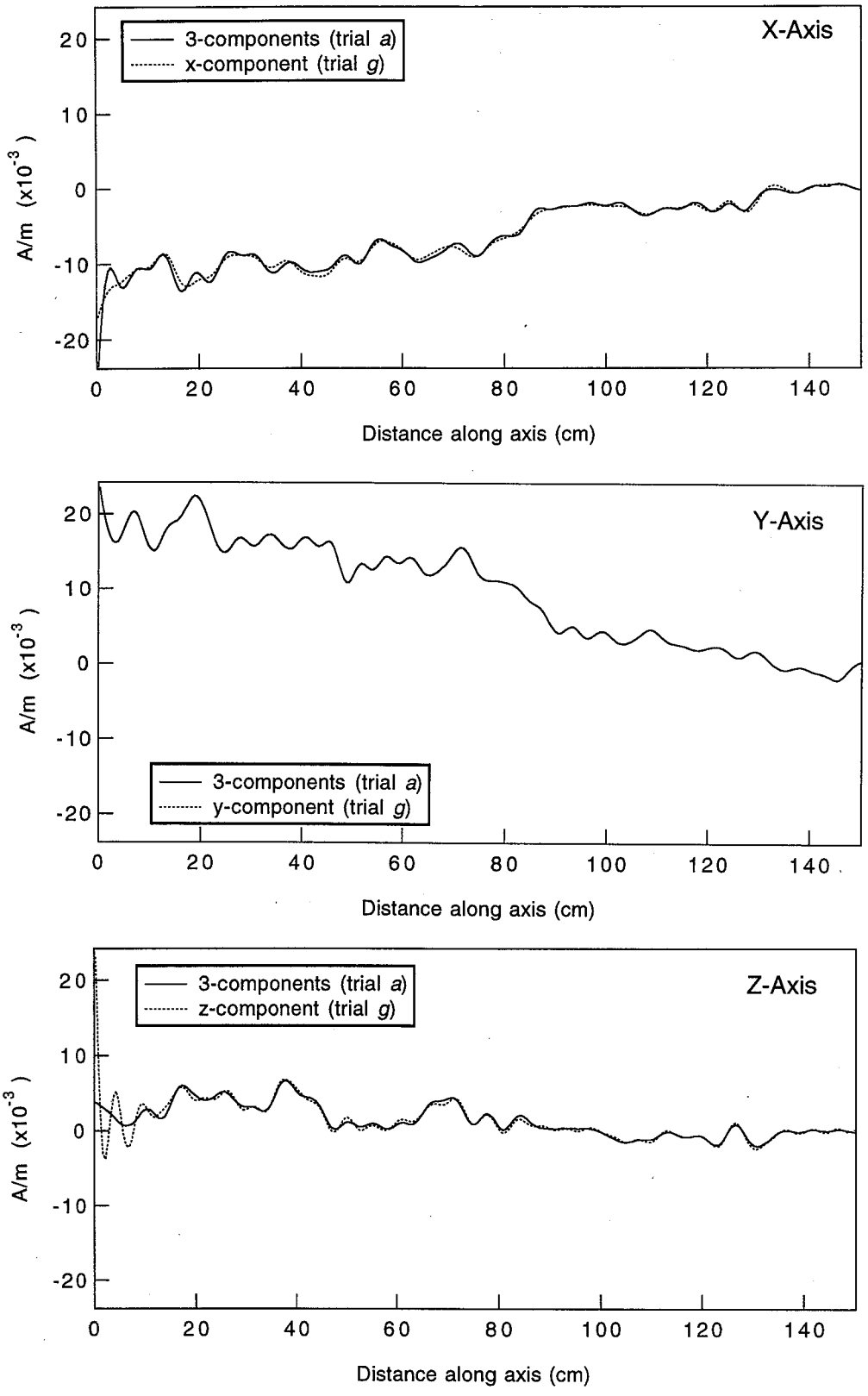

Figure 9. The deconvolved magnetizations for the measurements of Section 769B-7H6 at 20 mT AF demagnetization by the correct response curve are plotted by solid lines (trial a). The results of deconvolution separately conducted on the same data are plotted by dotted lines (trial g).

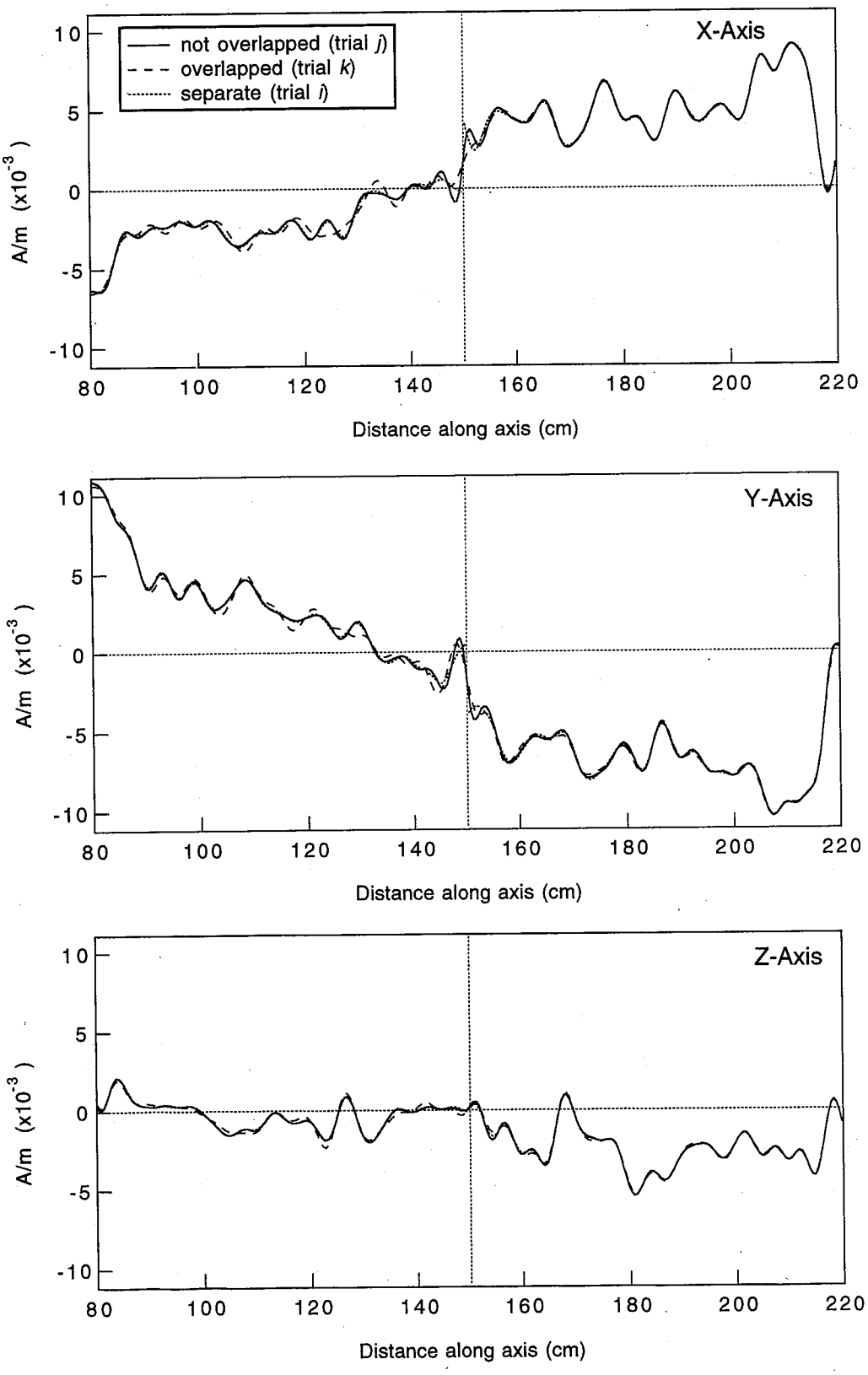

Figure 10. The deconvolved magnetizations for the measurements of Sections 769B-7H6 and 769B-7H7 at 20 mT AF demagnetization are plotted. The connection of two adjacent sections are demonstrated by separate deconvolution (dotted lines, trial i), overlapping deconvolution (dashed lines, trial k), and nonoverlapping deconvolution (solid lines, trial j).

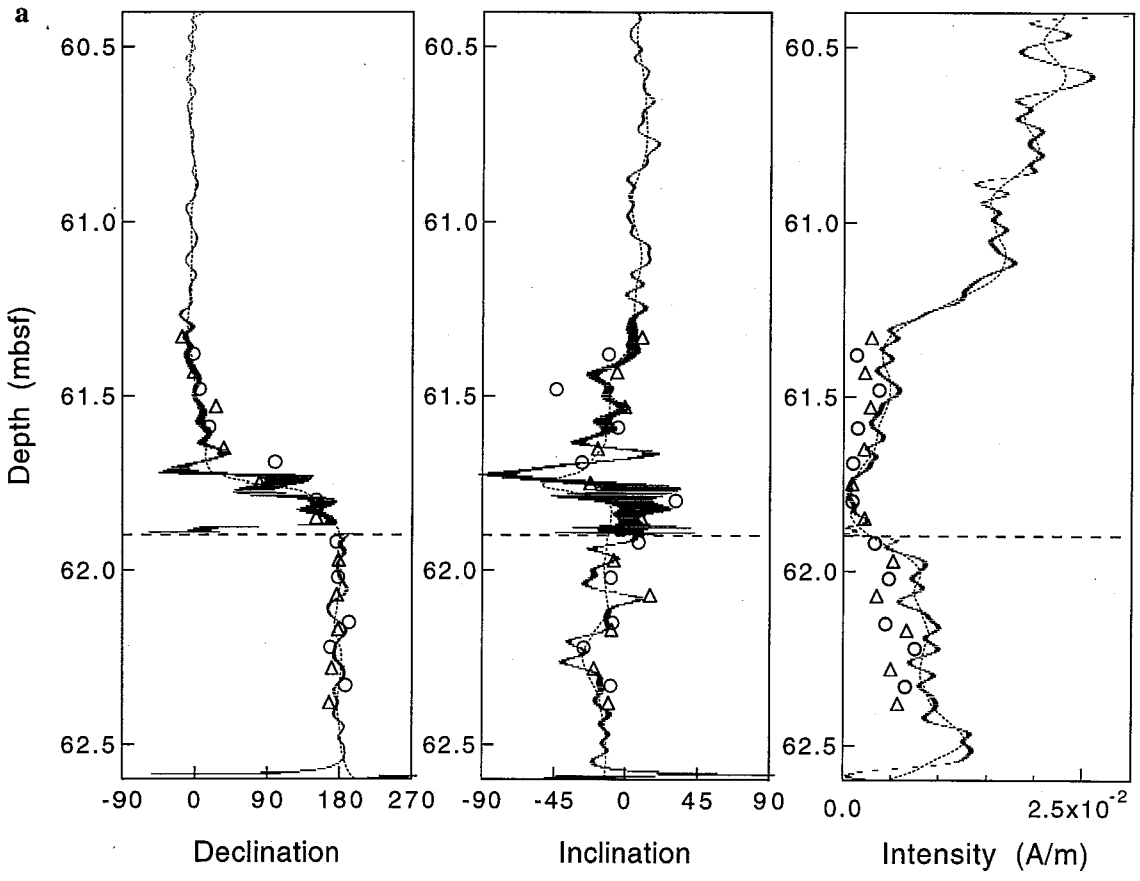

Figure 11. Declination, inclination and intensity for (a) Sections 769B-7H6 and 769B-7H7 (trial j) and (b) Sections 769A-7H4 and 769A-7H5 (trial o) are plotted versus depth in mbsf (meters below sea floor) for magnetization calculated without deconvolution (dashed lines) and magnetization after deconvolution (dots with horizontal bars representing 95% confidence limits). The magnetization measured on cube samples after alternating field demagnetization at 20 mT are shown by open circles and thermal demagnetization at 400°C by open triangles. The data of cube samples for Hole 769A are from *Schneider et al.* [1992].

results of deconvolution and the magnetizations of cube samples show important agreement, whereas the magnetizations after deconvolution differ from those before deconvolution. The slight discrepancy between the magnetizations after deconvolution and cube samples may come from heterogeneity of the samples, disturbances due to sampling and/or alteration of magnetization of cube samples during the time after the drilling.

How to Connect Adjacent Sections

In addition to deconvolution of separate sections, two ways of joining adjacent sections were demonstrated. The overlapping method (e.g., trial k) deconvolves the data as one succession, while another method (e.g., trial j) deconvolves by using a response matrix composed of two separate blocks of columns representing sensor responses. The former method draws curves more smoothly across the junction. However, minimum ABIC is slightly larger than that of the latter method and the magnetization shows meaningful discrepancy within 30 cm of the joint from the separately deconvolved results (e.g., trials a and h). On the other hand, the difference between trials i and j is very small except within about 5 cm of both sides of the junction. Under ideal conditions, these three results should be in agreement. The discrepancy may come from the disturbance of sediments on the cutting plane due to splitting and/or the initial heterogeneity of sediments. There may also be a possibility that the long-core is somewhat offset on the transporting plastic boat. In order to avoid effects both by disturbance of the sediments and by overrelaxation at the joint, the method which joints without overlapping the data was used. However, data points very close to the boundary of the sections (~2 cm) should be omitted especially in the case of low-intensity magnetization.

Noise Source and Resolution

There are several possible sources of noise in the pass-through measurements. These include electromagnetic noise, noise related to the positioning inaccuracy, lateral variation of the magnetization in the sample, and noise introduced from the empirical response as in (2).

The noise level of the SQUID system is inversely proportional to the square root of the frequency with low-pass filter and the noise for 1 Hz is calculated as 5.22×10^{-12}, 4.94×10^{-12}, and 6.74×10^{-12} (A m^2), in x, y, and z axis,

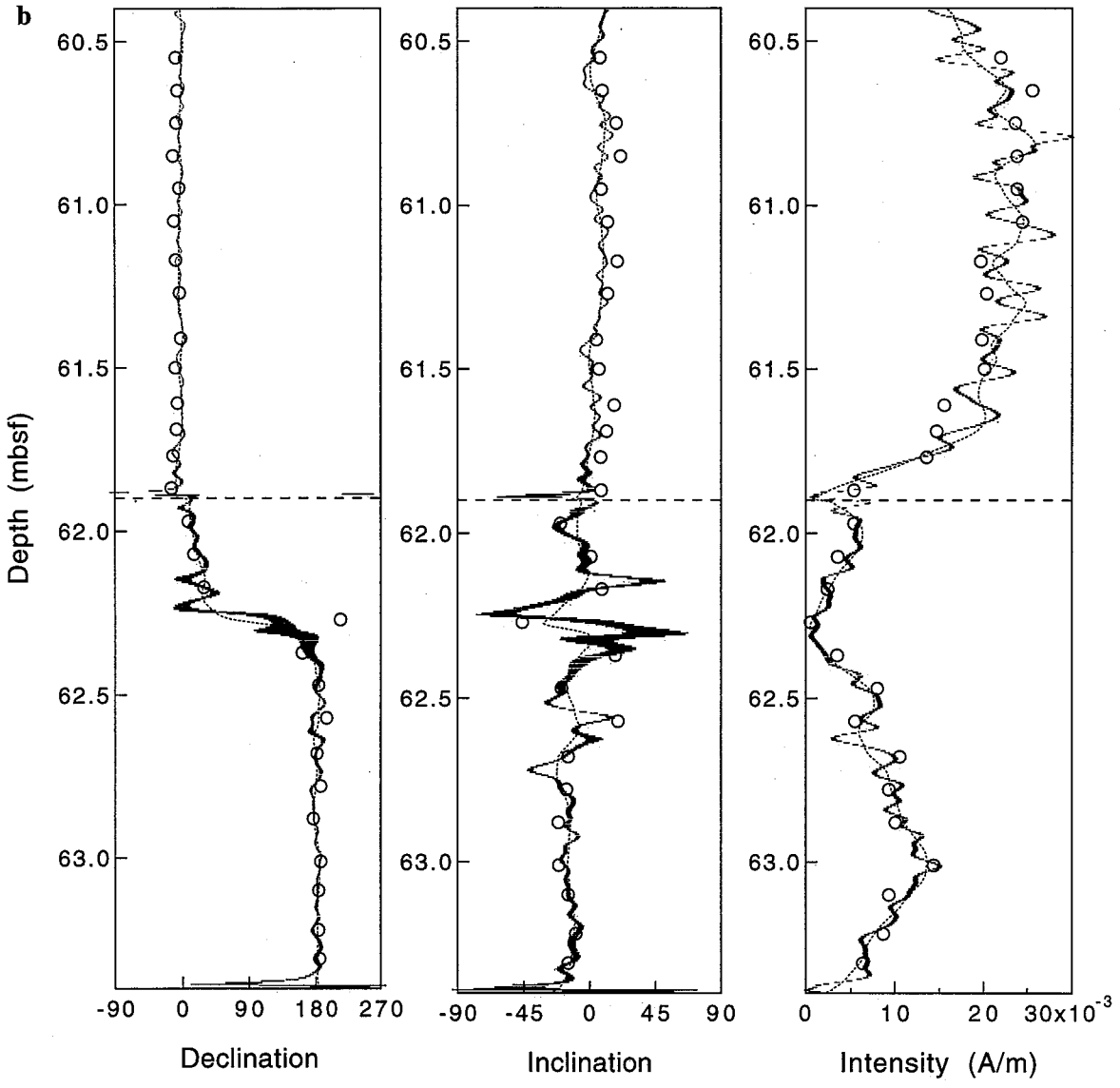

Figure 11. (continued)

respectively. The estimated noise level of the measurements is 3.6×10^{-9} A m^2, which is about 1000 times larger than the electromagnetic noise. Thus the electromagnetic noise is negligible compared to the total noise level except the formerly mentioned spike noises caused by other electronics.

Although the long core is transported by a stepping motor, the displacement from the proper position can possibly be introduced by an irregular extension of polyurethane rope due to the heavy weight of the long-core samples. The displacement may be a noise source in combination with the gradient of the magnetization at the point. The effect of random error in measurement positions can be detected by multiple measurements on the same core at the same demagnetization level. However, as the samples that we used were measured only once at each demagnetization step, the pass-through data at two different demagnetization steps were used for comparison. The residuals of deconvolution for the paleomagnetic data of two different AF demagnetization levels (15 and 20 mT) on section 124-769B-7H6 show a very similar pattern on a large scale (Figure 12). In both cases the residuals are composed of random noise and periodic waves of about 15 cm wavelength. These suggest that the residuals are not mainly produced by the source changeable from one measurement to another such as the electromagnetic noise or the positioning error. All the cores tested yielded similar results, which suggests that the source of periodic waves in the noise is principally due to noise in the response curves and/or lateral heterogeneity of the magnetization. The periodicity of the residuals suggests that the noise possibly comes from the response curves with systematic difference in shape (half width) [*Oda and Shibuya*, 1994] and/or the systematic distortion of the sediment resulting from the drilling process. Although the residual can be reduced further by using more accurate response curves, the resolution may finally be restricted by lateral heterogeneity of the sediment before encountering the limit of electromagnetic noise.

It can be expected that the outer part of the APC, as compared to the center of the core, is affected more by drilling disturbances. Thus the U-channel sampling from the center of the APC is desirable to reduce the lateral heterogeneity. The U-

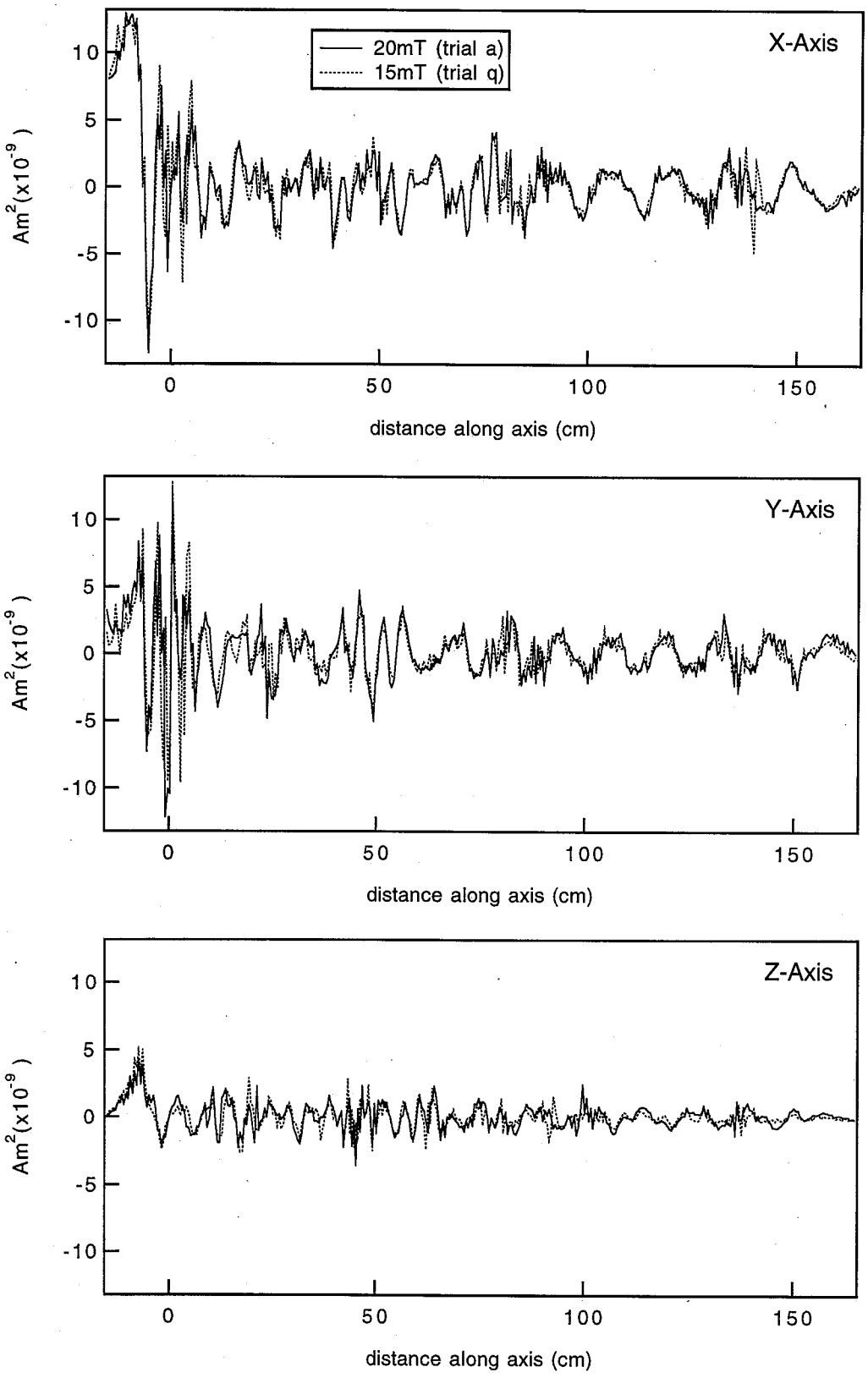

Figure 12. The residuals of deconvolution between the SQUID output and moment calculated from the model magnetization on Section 769B-7H6 for AF demagnetization of 20 mT (solid lines, trial a) and 15 mT (dashed lines, trial q). The dominant pattern is very similar to each other indicating that the contribution of positioning error (expected to be randomly distributed) to the noise may be trivial.

channel sampling technique reduces the disturbance from the outer part of the core and enhances the spatial resolution. However, this method is associated with another problem as the magnetization records tend to be affected by heterogeneity which may lead to the magnetization affected by local sediment artifacts such as bioturbation rather than the desired global paleomagnetic field record. To obtain reliable records of the paleomagnetic field, the sample must have a volume larger than the scale of the disturbance.

The important point is that the resolution of deconvolved magnetization cannot be significantly improved by reducing the measurement spacing or by reducing the noise level as has been suggested by *Constable and Parker* [1991]. They showed that spatial resolution of the magnetometer could be significantly enhanced by using smaller diameter pick-up coils for the measurement. A new high-resolution magnetometer with pick-up coils of small diameter (a modified 4.2 cm access model 755-R with two sets of SQUIDS) has recently been developed by 2G, which enabled us to measure U-channel samples with spatial resolution of 4 cm [*Nagy and Valet*, 1993; *Weeks et al.*, 1993]. Deconvolution of the data further increased the resolution to about 2 cm.

Although the SQUID magnetometer on board *Joides Resolution* has a significantly wide sensor response (~11 cm), it was possible to improve the resolution of the magnetization to a maximum of about 2 cm by deconvolution. With respect to our current use of the existing magnetometer for the measurement of the archive half, the deconvolution presented here can be an important tool to raise the resolution of the paleomagnetic records. One advantage of pass-through measurement on *Joides Resolution* is that the measurements are usually carried out within a day, typically several hours, after the recovery of the APC samples. This may rule out the possibility of alteration after the recovery of the samples. The deconvolution can be used in the initial scan for the records of geomagnetic reversals, especially short events and excursions which are hard to detect before deconvolution, and assessment for subsequent sampling. Likewise, the ABIC minimizing deconvolution is a powerful tool for the detailed study of geomagnetic secular variations because pass-through measurement may be the only way to obtain continuous records from ODP sediments due to its restricted sampling strategy.

Conclusions

The deconvolution by minimizing Akaike's Bayesian Information Criterion (ABIC) was developed for long-core paleomagnetic data of ODP sediments. The deconvolution scheme was applied to the pass-through data of APC samples from Holes 769A and 769B of Leg 124 measured at intervals of 5 mm and the resolution was improved from the spatial resolution of pick-up coils (~11 cm) to the spatial resolution of about 2 cm maximum. The magnetizations after the deconvolution are in favorable agreement with the magnetic remanence measured on the cube samples independently.

The noise estimation is quite consistent with the amplitude of noise added before deconvolution for the synthetic data. This ensures that the ABIC minimization deconvolution is reasonable as long as the assumption of Gaussian noise distribution holds. Various tests to confirm the accuracy of the response curves revealed that the old response is not applicable for the deconvolution. However, the role of the cross term appears to be insignificant with respect to the deconvolution.

Main noise sources of the pass-through data may be the lateral variation of the magnetization and noise in the empirical response curve. The noise of the empirical response curve can be reduced to some extent. However, the spatial resolution of the measurement is essentially limited by the lateral variation of the magnetization due to bioturbation and/or drilling disturbance. A recently developed magnetometer for U-channel samples with smaller diameter pick-up coils strongly enhanced the spatial resolution to about 4 cm [*Nagy and Valet*, 1993; *Weeks et al.*, 1993]. Although the new magnetometer is the powerful tool for detailed paleomagnetic study, the deconvolution scheme for the ODP pass-through measurement system presented here can play an important role in the detailed paleomagnetic study with its high productivity and prompt measurement free of alteration.

Acknowledgments. We thank the associate editor and referees for helpful and critical comments on the original manuscript. We appreciate Masayuki Torii for his constructive comments throughout the work. The final manuscript was greatly improved with the help of Jeff Michaelson. We are grateful to Dean Merrill and Vindell Hsü for their help on the pass-through measurements of APC samples, and Ulrike Körner for her help on the measurement of sensor response curves of the magnetometer. David Schneider kindly supplied the magnetic remanence data of cube samples from ODP Hole 769A. Catherine Constable and Robert Parker provided their extremely helpful deconvolution program. The samples were supplied with the permission of the Ocean Drilling Program. H.O. would like to acknowledge support from JSPS Fellowships for Japanese Junior Scientists. Additional support was provided by the Grant-in-Aid for Specially Promoted Research 04216105 from the Ministry of Education, Science, and Culture of Japan. The FORTRAN code of the deconvolution program is available upon request through e-mail at hoda@gsj.go.jp.

References

Akaike, H., Likelihood and the Bayes procedure, in *Bayesian Statistics*, edited by J. M. Bernardo, M. H. DeGroot, D. V. Lindley and A. F. M. Smith, pp. 143-166, Univ. Press, Valencia, Spain, 1980.

Akaike, H., On the selection of prior distribution and its application, in *Bayesian Statistics and Its Application (in Japanese)*, edited by Y. Suzuki and N. Kunitomo, pp. 81-98, Tokyo Univ. Press, Tokyo, 1989.

Constable, C., and R. Parker, Deconvolution of long-core palaeomagnetic measurements: Spline therapy for the linear problem, *Geophys. J. Int.*, *104*, 453-468, 1991.

Dimri, V., *Deconvolution and Inverse Theory, Application to Geophysical Problems*, Elsevier, New York, 1992.

Dodson, R., M. Fuller, and W. Pilant, On the measurement of the magnetism of long cores, *Geophys. Res. Lett.*, *1*, 185-188, 1974.

Murata, Y., Estimation of Bouguer reduction density using ABIC minimization method (in Japanese), *Seismology*, *43*, 327-339, 1990.

Nagy, E. A., and J.-P. Valet, New advances for paleomagnetic studies of sediment cores using *u*-channels, *Geophys. Res. Lett.*, *20*, 671-674, 1993.

Oda, H., and H. Shibuya, Deconvolution of whole-core magnetic remanence data by ABIC minimization, *J. Geomagn. Geoelectr.*, *46*, 613-628, 1994.

Okamoto, Y., *Inverse Problem and Its Solution (in Japanese)*, edited by T. Musha, Ohm, Tokyo, 1992.

Press, W. H., S. A. Teukolsky, W. T. Vetterling, and B. P. Flannery, *Numerical Recipes in Fortran, The Art of Scientific Computing*, 2nd ed., Cambridge Univ. Press, New York, 1992.

Rangin, C., et al., *Proceedings of the Ocean Drilling Program, Initial Reports*, vol. 124, Ocean Drilling Program, College Station, TX, 1990.

Schneider, D. A., D. V. Kent, and G. A. Mello, A detailed chronology of the Australasian impact event, the Brunhes-Matuyama

geomagnetic polarity reversal, and global climate change, *Earth Planet. Sci. Lett.*, *111*, 395-405, 1992.

Tamura, Y., T. Sato, M. Ooe, and M. Ishiguro, A procedure for tidal analysis with a Bayesian information criterion, *Geophys. J. Int.*, *104*, 507-516, 1991.

Tarantola, A., *Inverse Problem Theory, Methods for Data Fitting and Model Parameter Estimation*, Elsevier, New York, 1987.

Togawa, H., *Matrix Calculations* (*in Japanese*), Ohm, Tokyo, 1971.

Tsunakawa, H., Bayesian approach to smoothing palaeomagnetic data using ABIC, *Geophys. J. Int.*, *108*, 801-811, 1992.

Weeks, R., C. Laj, A, L. Endignoux, M. Fuller, A. Roberts, R. Manganne, E. Blanchard, and W. Goree, Improvements in long-core measurement techniques: Applications in palaeomagnetism and palaeoceanography, *Geophys. J. Int.*, *114*, 651-662, 1993.

H.Oda, Marine Geology Department, Geological Survey of Japan, 1-1-3 Higashi, Tsukuba 305, Japan. (e-mail: hoda@gsj.go.jp)

H. Shibuya, Department of Earth Science, College of Integrated Arts and Sciences, University of Osaka Prefecture, Sakai 591, Japan. (e-mail: a64246@center.osaka-u.ac.jp)

(Received February 10, 1995; revised August 23, 1995; accepted September 7, 1995.)